European Journal of Mechanics / B Fluids 79 (2020) 190–201

Contents lists available at ScienceDirect

European Journal of Mechanics / B Fluids

journal homepage: www.elsevier.com/locate/ejmflu

Uncertainty analysis of computed flow rates and pressure differences in rarefied pressure and temperature driven gas flows through long capillaries

Giorgos Tatsios *, Dimitris Valougeorgis

Department of Mechanical Engineering, University of Thessaly, 38334, Volos, Greece

ARTICLE INFO

Article history:
Received 29 May 2019
Received in revised form 6 August 2019
Accepted 13 September 2019
Available online 18 September 2019

Keywords:
Rarefied gas
Uncertainty propagation
Monte Carlo method
Poiseuille flow
Thermal transpiration
Thermomolecular pressure difference

ABSTRACT

The computation of the mass flow rate in the Poiseuille and thermal creep flows and of the pressure difference in the thermomolecular pressure difference (TPD) flow through long capillaries is well-known and available in the literature. Here, the uncertainty in the solution due to induced uncertainties in the input data, namely, the capillary radius and length, the pressure and/or temperature imposed at the capillary ends and the accommodation coefficient of the Maxwell diffuse-specular boundary conditions, is investigated. The uncertainty analysis is performed by the Monte Carlo Method. Conducting the required number of trials the distribution function of the output quantity and its associated uncertainty are obtained. In most cases, the uncertainty in the input quantity driving the flow has the largest effect on the output uncertainties. This is always true in the TPD flow and for small pressure and temperature differences in the Poiseuille and thermal creep flows respectively. In the case of large driving thermodynamic forces, in the latter two flows, the radius becomes the most important source of uncertainty. The accommodation coefficient uncertainty is always the less important one. Documenting the expected effect of the uncertainty in each input parameter is certainly beneficial in computational as well as experimental work.

1. Introduction

In rarefied gas dynamics, as in any number of fields, uncertainties arise both in computational and experimental work. The uncertainties may be introduced through the input data or generated during the development of the task. Then, they propagate along the implemented process and they finally appear at the output computed or measured quantities. Depending on various parameters the uncertainties in the output quantities, compared to the input ones, may be of the same order or either increased or decreased.

In typical computational fluid dynamics uncertainties are introduced due to the assumptions and simplifications in the physical and mathematical modeling, the discretization of the problem, the boundary conditions, the floating point operations and others [1–3]. Similarly, in experimental work, uncertainties are introduced due to various sources, such as the specifications of the measuring instruments, the changing environmental conditions, the estimation of the quantity of interest in an indirect manner through some other measured quantity and some expression connecting the two quantities (e.g. mass flow rate through pressure), which may involve approximations and the flaws in the experimental setup resulting to significant variations in repeated measurements [4–6].

In rarefied gas dynamics, uncertainties are introduced due to all above causes, as well as due to additional factors such as the small geometrical sizes, low operating pressures and the unknown type of gas–surface interaction. Concerning experimental work, sensitivity analysis of the measured quantities is commonly performed. The uncertainty in the measured mass flow and pressure difference of rarefied gas flows through microchannels, due to the input data uncertainties, has been provided in several experimental works [7–10]. In addition, combining experimental and computational work the tangential momentum accommodation coefficients with their associated uncertainties for various gases and surfaces have been reported in [11].

Concerning computational work in rarefied gas dynamics, although documenting the uncertainty in the output quantities with regard to the uncertainty in the input data, should be valuable, in order to judge their expected validity and accuracy, only a limited number of systematic studies have been reported. Uncertainty quantification has been examined in microscale squeeze film damping [12] and in sharp leading-edge

* Corresponding author.
E-mail addresses: tatsios@mie.uth.gr (G. Tatsios), diva@mie.uth.gr (D. Valougeorgis).

https://doi.org/10.1016/j.euromechflu.2019.09.009
0997-7546/

hypersonic flows [13,14]. Also, uncertainty analysis has been performed in the computation of the flow field in the neutrino mass KATRIN experiment [15], as well as in metrology under low pressure conditions, in the computation of the effective areas of piston gauges [16,17]. Furthermore, a more detailed uncertainty assessment has been considered in the friction factor for flow through microchannels in the slip regime [18–20]. As far as the authors are aware of, no other systematic investigations are available in the literature. Computing the expected output uncertainties in various flow setups is obviously crucial for robust modeling and simulation, but also beneficial in the design of experimental rigs and devices by identifying favorable measurement conditions and process specifications respectively.

In general, the effect of the uncertainties in the input quantities or in the uncertainties generated during the task implementation, on the uncertainty in the output quantity is called uncertainty propagation. Several methods have been reported for uncertainty propagation [21,22]. The most notable ones include the interval analysis [23], the sensitivity derivatives [24], the moment methods [25], the polynomial chaos decomposition [26] and the Monte Carlo Method (MCM) [21,27]. The latter approach is considered as general, robust and accurate, requiring however high computational cost.

Based on all above, in the present work, the uncertainty propagation in the classical pressure and temperature driven flows through long tubes [28] is considered. More specifically, the effect of uncertainty in the input parameters (radius and length of the tube, pressure and temperature at the tube ends and accommodation coefficient of the Maxwell boundary conditions) on the uncertainty in the output mass flow rate and pressure difference is examined in a systematic manner. The specific flow setups include the Poiseuille flow [28], the thermomolecular pressure difference (TPD) [29] and the thermal creep flows [29], which are encountered in numerous technological applications including vacuum pumping systems [30,31], porous media [32] and gaseous microfluidics [33–35]. The uncertainty analysis is performed via the MCM, which is considered as suitable for the present work, since no model assumptions are needed and may be applied to models involving the solution of differential equations.

The rest of the paper is structured as follows. The kinetic formulation of the fully developed flows and the uncertainty propagation analysis are given in Sections 2 and 3 respectively. The computed results of uncertainty in the output quantities are presented in Section 4, which includes subsections 4.1, 4.2 and 4.3 associated to the Poiseuille, TPD and thermal creep flows respectively. The main concluding remarks are outlined in Section 5.

2. Flow configuration and kinetic formulation

Consider a long tube of length L and radius R, with $R \ll L$, connecting two vessels A and B, maintained at pressures P_A, P_B ($P_A \geq P_B$) and temperatures T_A, T_B ($T_A \leq T_B$). Along the tube wall a linear temperature distribution between the temperatures of the two vessels is applied. The vessels and the tube are filled with a rarefied monatomic gas. Due to the imposed pressure difference between the tube ends and temperature variation along the tube wall, pressure and thermally driven flows are induced, which correspond to the well-known cylindrical Poiseuille ($P_A > P_B$, $T_A = T_B$) [28] and thermal creep ($P_A = P_B$, $T_A < T_B$) flows respectively [29]. In addition, in the special case of zero net mass flow rate, the TPD flow is induced ($T_A < T_B$, $P_A < P_B$) [29]. The computational solution of these fully-developed rarefied gas flow problems in the whole range of the Knudsen number has been extensively investigated and is available in the literature. Here, we are interested in the uncertainty in the solution due to the uncertainties which are introduced in the input quantities. The uncertainties in the input data propagate through the computational model and they finally appear in the computational results of practical interest.

By superimposing the pressure and temperature driven flows, the mass flow rate $\dot{m}$ and pressure distribution $P(z)$ along the tube may be obtained by solving the first-order ordinary differential equation [29,36,37]

$$\frac{dP(z)}{dz} = -\frac{\upsilon_0(z)}{\pi R^3 G_P(\delta,\alpha)}\dot{m} + \frac{P(z)}{T(z)}\frac{G_T(\delta,\alpha)}{G_P(\delta,\alpha)}\frac{dT(z)}{dz} \tag{1}$$

along the tube axis $z \in [0, L]$, subject to boundary conditions $P(0) = P_A$ and $P(L) = P_B$. Here, $T(z) = T_A + (T_B - T_A)z/L$ is the known temperature distribution along the tube wall and $\upsilon_0 = \sqrt{2R_g T}$ is the most probable molecular speed at temperature T with R_g denoting the specific gas constant. Also, $G_P(\delta,\alpha)$ and $G_T(\delta,\alpha)$ are the dimensionless flow rates (also known as kinetic coefficients) for the pressure and temperature driven flows respectively [28,29,37] and they depend on the local gas rarefaction parameter $\delta(z) \in [0,\infty]$ and the gas-surface accommodation coefficient $\alpha \in [0, 1]$. The local gas rarefaction parameter is given by

$$\delta(z) = \frac{P(z)R}{\mu(z)\upsilon_0(z)}, \tag{2}$$

where $\mu(z)$ denotes the local viscosity which is given in terms of the inlet conditions as $\mu(z) = \mu_A\sqrt{T(z)/T_A}$, assuming hard-sphere interaction. The accommodation coefficient α, implemented in the diffuse-specular Maxwell boundary conditions, is denoting the percentage of particles undergoing diffuse reflection. The limiting values of $\alpha = 0$ and $\alpha = 1$, correspond to purely specular and purely diffuse reflection respectively. The coefficients G_P and G_T in terms of δ and α are obtained from the solution of the linearized Shakhov model equation [37] and the corresponding results are available in [28,29,37]. The Shakhov model and the Maxwell diffuse-specular boundary conditions have been chosen since they are most commonly implemented in the simulation of pressure and temperature driven gas flows through long capillaries providing reliable results in the whole range of gas rarefaction [16,38] with modest computational effort. In flow setups where more advanced kinetic modeling [39] is needed the present analysis may also be applied with increased computational effort.

Provided that the pressures P_A and P_B are given, Eq. (1) is solved using a shooting method in order to find the mass flow rate $\dot{m}$ and the pressure distribution $P(z)$. Alternatively, in cases where the mass flow rate $\dot{m}$ and one of the two pressures P_A or P_B are given, Eq. (1) is directly integrated via a Runge Kutta scheme to obtain the pressure distribution $P(z)$ including the second unknown pressure. Three types of flow, namely the Poiseuille flow [28,37], the thermomolecular pressure difference (TPD) flow [29] and the thermal creep flow [29,33,37], are considered.

The Poiseuille flow is driven only by the imposed pressure gradient, while the tube wall is assumed isothermal, i.e., $T(z) = T_A$ and $dT/dz = 0$. Then, Eq. (1) is reduced to

$$\frac{dP(z)}{dz} = -\frac{\upsilon_0}{\pi R^3 G_P(\delta,\alpha)}\dot{m} \tag{3}$$

subject to $P(0) = P_A$ and $P(L) = P_B$, which is solved by a shooting method to find $\dot{m}$ and $P(z)$. In this flow setup $\upsilon_0(z) = \upsilon_0(0)$, $\mu(z) = \mu(0)$ and $\delta(z) = \delta_A P(z)/P_A$.

The TPD flow is driven both by the imposed temperature gradient and the deduced pressure gradient, producing a flow in the opposite direction, with the overall net mass flow rate being equal to zero. By setting $\dot{m} = 0$, Eq. (1) is reduced to

$$\frac{dP(z)}{dT} = \frac{P(z)}{T(z)}\frac{G_T(\delta,\alpha)}{G_P(\delta,\alpha)} \tag{4}$$

subject to $P(0) = P_A$, which is directly integrated to find $P(z)$ and more importantly the pressure difference $\Delta P = P(L) - P(0)$.

Finally, the thermal creep flow is driven by the imposed temperature gradient along the tube, while the inlet and outlet pressures are maintained equal to each other, i.e., $P_A = P_B$. Although the two end pressures are equal, there is a pressure variation along the tube and therefore, a pressure driven flow is also deduced. Thus, Eq. (1) is solved in its original form subject to $P(0) = P(L) = P_A$, which is solved by a shooting method to find $\dot{m}$ and $P(z)$.

Solving either of Eqs. (1), (3) or (4), the kinetic coefficients G_P and G_T are always accordingly updated along the tube based on the local values of δ estimated by Eq. (2), using the local value of pressure, which is computed at each integration step and of temperature, which is given. The gas rarefaction parameter δ_A, at $z = 0$, is taken as reference.

In all cases the main input quantities, involved in the computation of the mass flow rates and the pressure distributions, include the length L and the radius R of the tube, the pressure and temperature at the tube ends P_A, P_B and T_A, T_B respectively and the accommodation coefficient α. All other quantities involved in the simulations, such as the kinetic coefficients, the local gas rarefaction parameter, as well as the viscosity and the most probable molecular speed of the working gas are expressed in terms of the main input data. Obviously, the uncertainties introduced in the main input quantities, will propagate through the computation scheme and will affect the output quantities. The uncertainty in the output quantities may be reduced, or be of the same order, or, more importantly, be magnified, compared to the uncertainty in the input quantities. The implemented uncertainty analysis is presented in the next section.

3. Uncertainty analysis

Let an input quantity be denoted as x_m, $m = 1, 2, \ldots, M$, with M being the number of input quantities. The nominal value of an input quantity and the associated uncertainty are denoted by $x_{m,n}$ and $u(x_m)$ respectively. Thus, any input quantity can be defined as $x_m = x_{m,n} \pm u(x_m)$. The output quantity is denoted by y and is a function of the input quantities x_m, i.e., $y = f(x_1, x_2, \ldots, x_M)$, while the associated uncertainty is $u(y)$. The objective is to document the uncertainty $u(y)$ of the output quantity y, based on the uncertainties $u(x_m)$ of the input quantities x_m as they propagate through the computational model $y = f(x_1, x_2, \ldots, x_M)$.

The uncertainty propagation analysis is performed using the Monte Carlo Method (MCM) [40,41]. The MCM is a stochastic method, according to which a large number of trials $i = 1, 2, \ldots, N_t$ is carried out. For each trial, the values of the input quantities that are subject to uncertainty are sampled from their respective distributions and a value for the output quantity is found. After the required number of trials is carried out, the distribution function of the output quantity is obtained and its associated uncertainty is calculated.

The uncertainty of the output quantity is usually defined as the 95% or the 99% coverage interval and it is estimated using the standard deviation of the output quantity distribution function [41], which is obtained using the MCM. The output quantity is presented in terms of the mean value and the associated uncertainty as

$$y = \bar{y} \pm u(y), \tag{5}$$

where the mean value is

$$\bar{y} = \frac{1}{N_t} \sum_{i=1}^{N_t} y_i \tag{6}$$

with y_i denoting the output of the ith trial and the associated uncertainty is

$$u(y) = k\sigma_y, \tag{7}$$

with the standard deviation given by

$$\sigma_y = \sqrt{\frac{1}{N_t - 1} \sum_{i=1}^{N_t} (y_i - \bar{y})^2}. \tag{8}$$

The coefficient k in Eq. (7) is the coverage factor and common values are $k = 2$ and $k = 3$ for the 95% and 99% coverage intervals respectively [40]. These values are used when a sufficient number of trials is performed (e.g., $N_t \approx 10^3$), while for smaller number of trials the coefficient k is taken from the Student distribution with N_t degrees of freedom. It is noted that using Eq. (8) along with the aforementioned values of k is a conservative approach that slightly overestimates the output uncertainty compared to finding the uncertainty from the discrete form of the output cumulative distribution function. This is done in order to account for the relative small number of trials conducted.

The input quantities as well as their uncertainty are usually known and are reported as $x_m = x_{m,n} \pm u(x_m)$, while the distribution of the input quantities is not always known. In cases where the form of the distribution is known, the value of x_m used in each trial is sampled from its respective distribution. In the general case, where this distribution is not known, a uniform distribution is assumed [41] between $x_m \in \left[x_{m,n} - u(x_m), x_{m,n} + u(x_m)\right]$ and the value for each trial is sampled from this distribution as $x_m = x_{m,n} + u(x_m)\left(1 - 2R_f\right)$, where R_f is a random number between 0 and 1. In the present work, a sufficient number of trials is performed and all input quantities are assumed to follow uniform distributions.

Furthermore, all uncertainties in the input and output quantities are reported as relative uncertainties defined as

$$\frac{u(x_m)}{x_m} \times 100\% \quad \text{and} \quad \frac{u(y)}{y} \times 100\%. \tag{9}$$

It is noted, that the effect of the uncertainty in each input quantity is considered individually. When one of the input quantities is subject to uncertainty, the uncertainties of all other input quantities are assumed to be zero. This way the effect that each input quantity has on the uncertainty in the output quantity of interest is separately obtained and a comparison between the effects of each input quantity is allowed. The combined uncertainty $u_c(y)$ of the output quantity when more than one input quantities x_m with the associated uncertainties $u(x_m)$ are considered, may be calculated as [40,41]

$$u_c(y) = \sqrt{\sum_{m=1}^{M} \left(u_{x_m}(y)\right)^2} \tag{10}$$

where $u_{x_m}(y)$ is the uncertainty in the quantity y due to the uncertainty in the input quantity x_m. Eq. (10) is valid when the input quantities are uncorrelated.

4. Results and discussion

The above described methodology is applied to the pressure and temperature driven flows through long tubes to compute the uncertainty in the output quantities. More specifically, the uncertainty in the output quantity of interest, i.e., of either the mass flow rate or the pressure difference, due to the uncertainties in the main input data, namely the uncertainties in pressure $u(P)$, temperature $u(T)$, radius $u(R)$, length $u(L)$ and accommodation coefficient $u(\alpha)$ is obtained. In subsections 4.1, 4.2 and 4.3 the Poiseuille, TPD and thermal creep flows with their associated

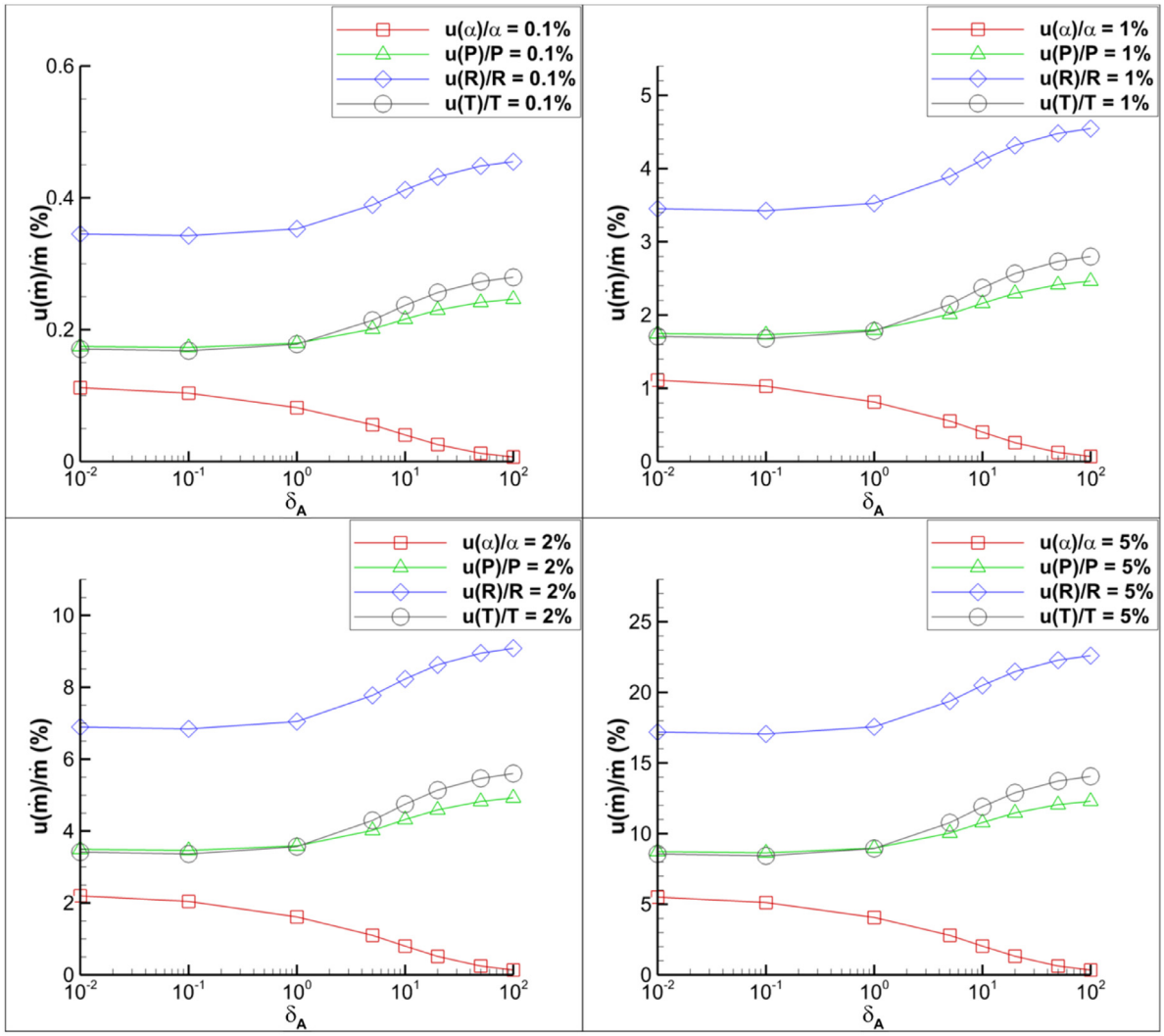

Fig. 1. Uncertainty $u(\dot{m})/\dot{m}$ of the output mass flow rate in the Poiseuille flow in terms of δ_A, with the uncertainty in the input quantities of radius $u(R)/R$, pressure $u(P)/P$, temperature $u(T)/T$ and accommodation coefficient $u(\alpha)/\alpha$ equal, in each case, to 0.1%, 1%, 2% and 5%.

input and output uncertainties are respectively considered. In each flow configuration $N_t = 10^3$ trials are conducted, while in each trial a value for the input quantity subject to uncertainty is sampled from a uniform distribution. Then, solving the corresponding model equation, i.e., Eq. (1), (3) or (4), the discrete form of the output quantity distribution function is recovered, which is used to calculate the respective uncertainty. The results include only the uncertainties and not the distributions themselves, since they are not of practical interest and they are always given in terms of the rarefaction parameter at the inlet (δ_A) calculated through Eq. (2) using the nominal values of the parameters at $z = 0$. Also, all reported values of the output quantity uncertainty correspond to 95% coverage intervals. The values of the relative uncertainty in the input quantities are chosen to be 0.1%, 1%, 2% and 5% in order to investigate the behavior of the relative uncertainty in the output quantity in terms of the input ones.

4.1. Uncertainty of mass flow rate in Poiseuille flow

The purely pressure driven Poiseuille flow, based on Eq. (3), is first considered. Simulations are conducted in a wide range of the reference rarefaction parameter δ_A, ranging from the free molecular up to the continuum regimes. The effect of the uncertainties in the main input quantities of pressure, temperature, radius, length and accommodation coefficient on the uncertainty $u(\dot{m})/\dot{m}$ of the produced mass flow rate is analyzed. Furthermore, the effect of the pressure ratio driving the flow on the mass flow rate uncertainty is considered. It is noted that in the Poiseuille flow, the inlet and outlet pressures P_A and P_B respectively, are subject to the same level of uncertainty and their respective values are sampled individually.

The effect of the relative uncertainty $u(L)/L$ of the input length on the mass flow rate, unlike all other input parameters, may be analytically treated. Considering Eq. (3) and utilizing the sensitivity derivatives approach [40], it is readily deduced that the relative uncertainty in the mass flow rate due to uncertainties in the tube length may be written in a closed form as

$$\frac{u(\dot{m})}{\dot{m}} = \frac{u(L)}{L}. \tag{11}$$

It is clearly seen that the output uncertainty is of the same order of the input one. It is also noted that for long capillaries, length measurements typically have, compared to the other parameters, small measurement uncertainty.

Next, based on the uncertainty analysis described in Section 3, the uncertainty $u(\dot{m})/\dot{m}$ of the output mass flow rate in terms of δ_A is plotted in Fig. 1 for four values of the relative uncertainty in all other main input quantities. More specifically, the presented results are for the input quantities of pressure, temperature,

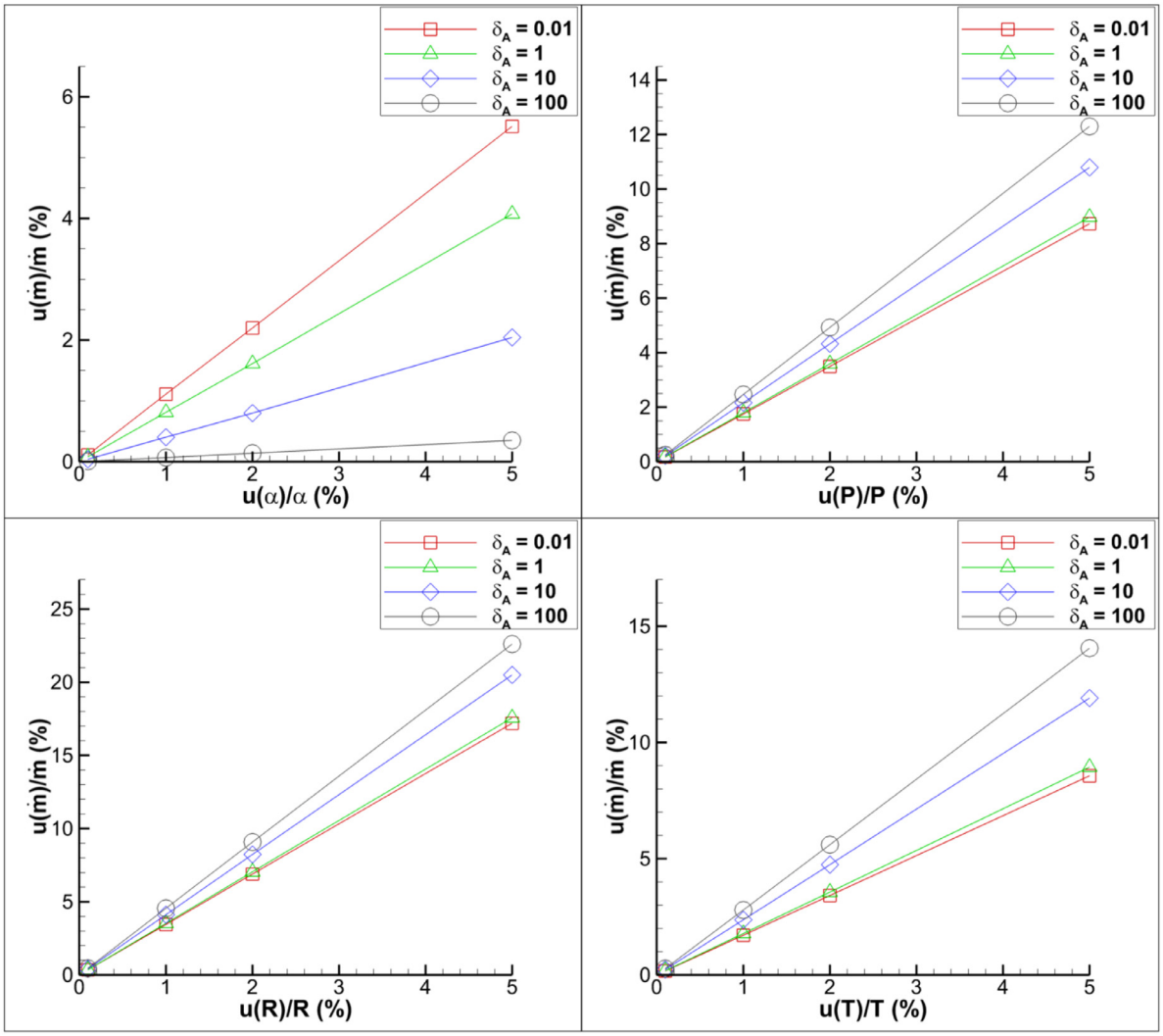

Fig. 2. Uncertainty $u(\dot{m})/\dot{m}$ of the output mass flow rate in the Poiseuille flow in terms of $u(\alpha)/\alpha$, $u(P)/P$, $u(R)/R$ and $u(T)/T$ for $\delta_A = 0.01$, 1, 10 and 100.

radius and accommodation coefficient with the associated uncertainties $u(P)/P$, $u(T)/T$, $u(R)/R$ and $u(\alpha)/\alpha$ respectively, taking in each case the values of 0.1%, 1%, 2% and 5%. The ratio of the length over the nominal radius of the tube is $L/R_n = 20$, the ratio of the nominal pressures at $z = 0$ and $z = L/R_n$ driving the flow is $P_{B,n}/P_{A,n} = 0.5$ and the nominal accommodation coefficient is $\alpha_n = 1$.

In all cases, larger uncertainties in the input quantities lead to larger uncertainties in the mass flow rate, observing for all values of each input uncertainty the same qualitative behavior. The radius, temperature and pressure uncertainties affect significantly the mass flow rate uncertainty in the whole range of the gas rarefaction parameter δ_A. For $\delta_A \leq 1$, the uncertainty in the mass flow rate due to the uncertainties in P, R and T, remains almost constant and then, for $\delta_A > 1$ exhibits a slight increase. The effect of the accommodation coefficient uncertainty α is important only for $\delta_A \leq 1$ and then as δ_A is increased, its effect is decreased becoming negligible in the slip and continuum regimes. In all flow regimes, the radius uncertainty has clearly the most significant effect on the mass flow rate uncertainty, followed by the pressure and temperature uncertainties which have about the same effect. It is seen that $u(\dot{m})/\dot{m}$ is magnified more than three times compared to $u(R)/R$ and about two times compared to $u(P)/P$ and $u(T)/T$. Finally, the effect of the uncertainty in the accommodation coefficient of the Maxwell boundary conditions for $\alpha_n = 1$, is the smallest one in all flow regimes and $u(\dot{m})/\dot{m}$ is always equal or smaller than $u(\alpha)/\alpha$. The maximum values of the mass flow rate uncertainties for 5% uncertainty in radius, temperature, pressure and accommodation coefficient, are about 22%, 14%, 12% and 5% respectively.

Based on the results of Fig. 1, it may be deduced that $u(\dot{m})/\dot{m}$ grows linearly with all input relative uncertainties. This is clearly demonstrated in Fig. 2, where the relative uncertainty in the mass flow rate $u(\dot{m})/\dot{m}$ is given in terms of the relative uncertainties in accommodation coefficient $u(\alpha)/\alpha$, pressure $u(P)/P$, tube radius $u(R)/R$ and temperature $u(T)/T$ for various values of δ_A, with $L/R_n = 20$, $P_{B,n}/P_{A,n} = 0.5$ and $\alpha_n = 1$. This observation remains valid for all input parameters, within the examined range of their relative uncertainty.

Since the Poiseuille flow is a pressure driven flow, it is important to investigate in detail the effect of the input pressure ratio $P_{B,n}/P_{A,n}$ on the mass flow rate uncertainty due to the uncertainty in the input pressures. In Fig. 3, the uncertainty $u(\dot{m})/\dot{m}$ of the mass flow rate in terms of δ_A is plotted for nominal pressure ratios $P_{B,n}/P_{A,n} = 0.3$, 0.5, 0.7 and 0.9, with the input uncertainty in pressure $u(P)/P$ taking the values of 0.1%, 1%, 2% and 5%. The dimensionless length and the accommodation coefficient are as before ($L/R_n = 20$ and $\alpha_n = 1$). As the nominal pressure ratio increases, i.e., the pressure difference decreases, the uncertainty in the mass flow rate due to the input pressure uncertainty is significantly increased. The values of the mass flow rate uncertainty

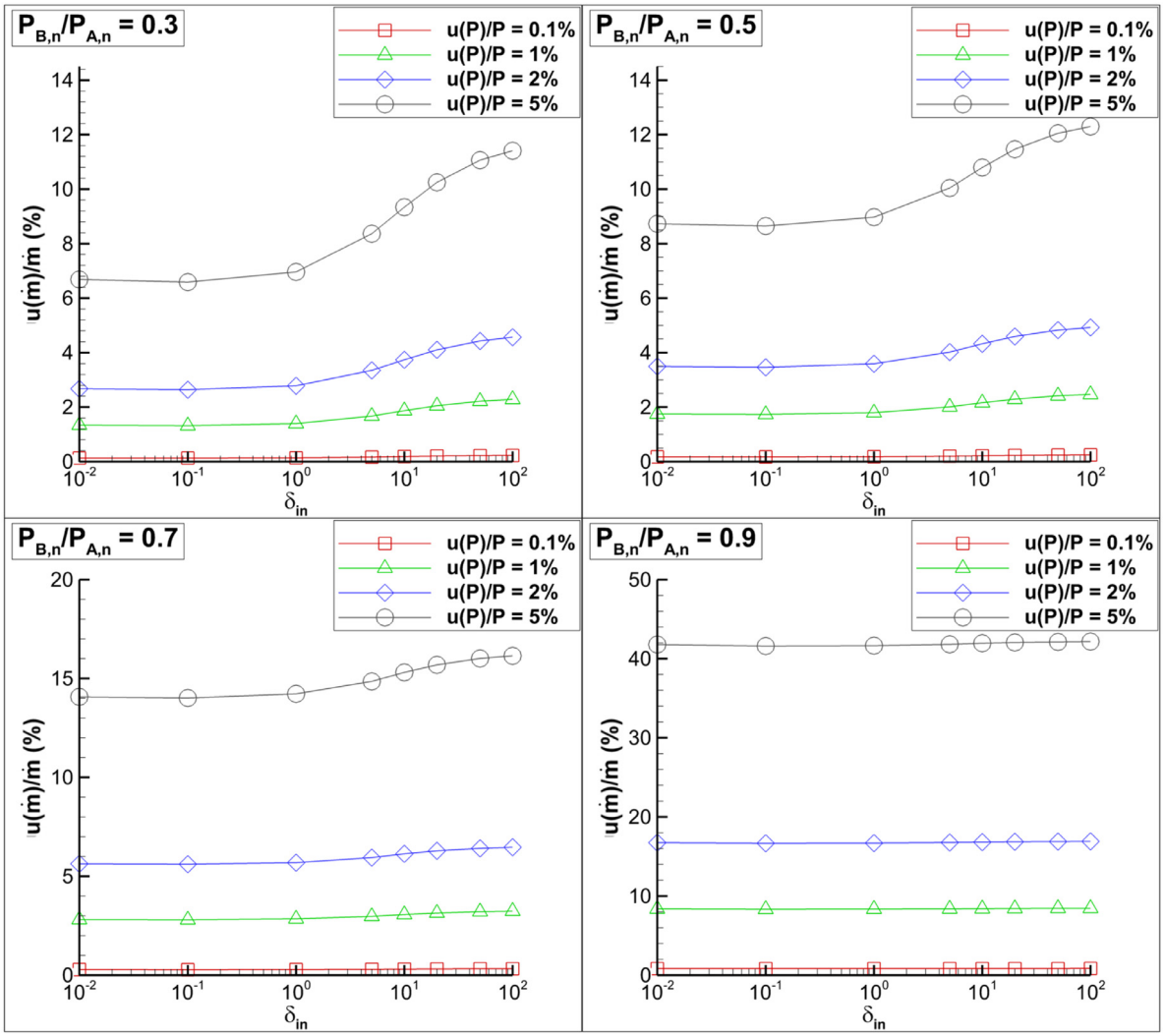

Fig. 3. Uncertainty $u(\dot{m})/\dot{m}$ of the output mass flow rate in the Poiseuille flow in terms of δ_A for $P_{B,n}/P_{A,n} = 0.3$, 0.5, 0.7 and 0.9, with the uncertainty in the input pressure $u(P)/P = 0.1\%$, 1%, 2% and 5%.

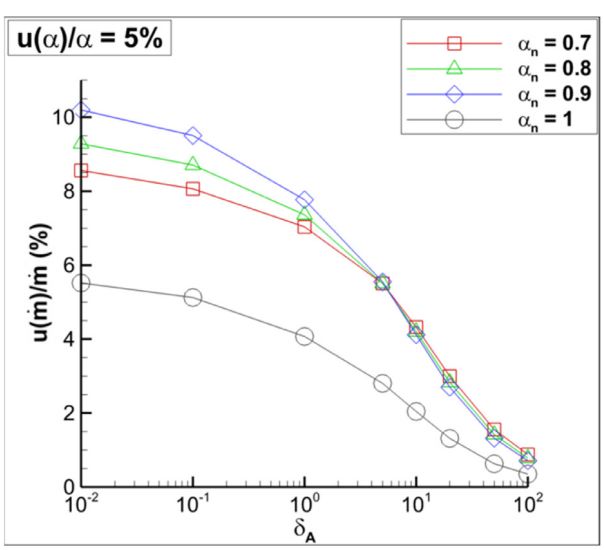

Fig. 4. Uncertainty $u(\dot{m})/\dot{m}$ of the output mass flow rate in the Poiseuille flow in terms of δ_A for $\alpha_n = 0.7$, 0.8, 0.9 and 1, with the uncertainty in the accommodation coefficient $u(\alpha)/\alpha = 5\%$.

for 5% uncertainty in pressure reach up to 11%, 12%, 16% and 42% for pressure ratios 0.3, 0.5, 0.7 and 0.9 respectively. It is seen that for pressure ratio 0.9, the pressure uncertainty becomes the dominant factor of the mass flow rate uncertainty. Overall, it may be stated that in the Poiseuille flow the output mass flow rate uncertainty is mostly affected by the input radius and pressure uncertainties in large and small pressure differences respectively.

In Fig. 4, the mass flow rate uncertainty due to the uncertainty in the accommodation coefficient for $\alpha_n \leq 1$ is investigated. It is seen that $u(\dot{m})/\dot{m}$ for $\alpha_n < 1$ is roughly doubled compared to the corresponding one for $\alpha_n = 1$. This is expected, since in purely diffuse accommodation any time that a value larger than one, according to the general definition $\alpha = 1 \pm u(\alpha)$ is sampled, is discarded as unphysical and a new value is sampled in order always to be less or equal to one. Furthermore, comparing the results between different values of $\alpha_n < 1$ it is seen that in the free molecular and transition regimes the mass flow rate uncertainty is slightly reduced as the reflection becomes more specular, while in the slip and viscous regimes very small deviations between the different values of $\alpha_n < 1$ are observed. The described overall behavior of $u(\dot{m})/\dot{m}$ with respect to input uncertainties $u(\alpha)/\alpha$ for $\alpha_n \leq 1$ in the Poiseuille flow, also appears in the computed output quantities of the thermal creep and TPD flows.

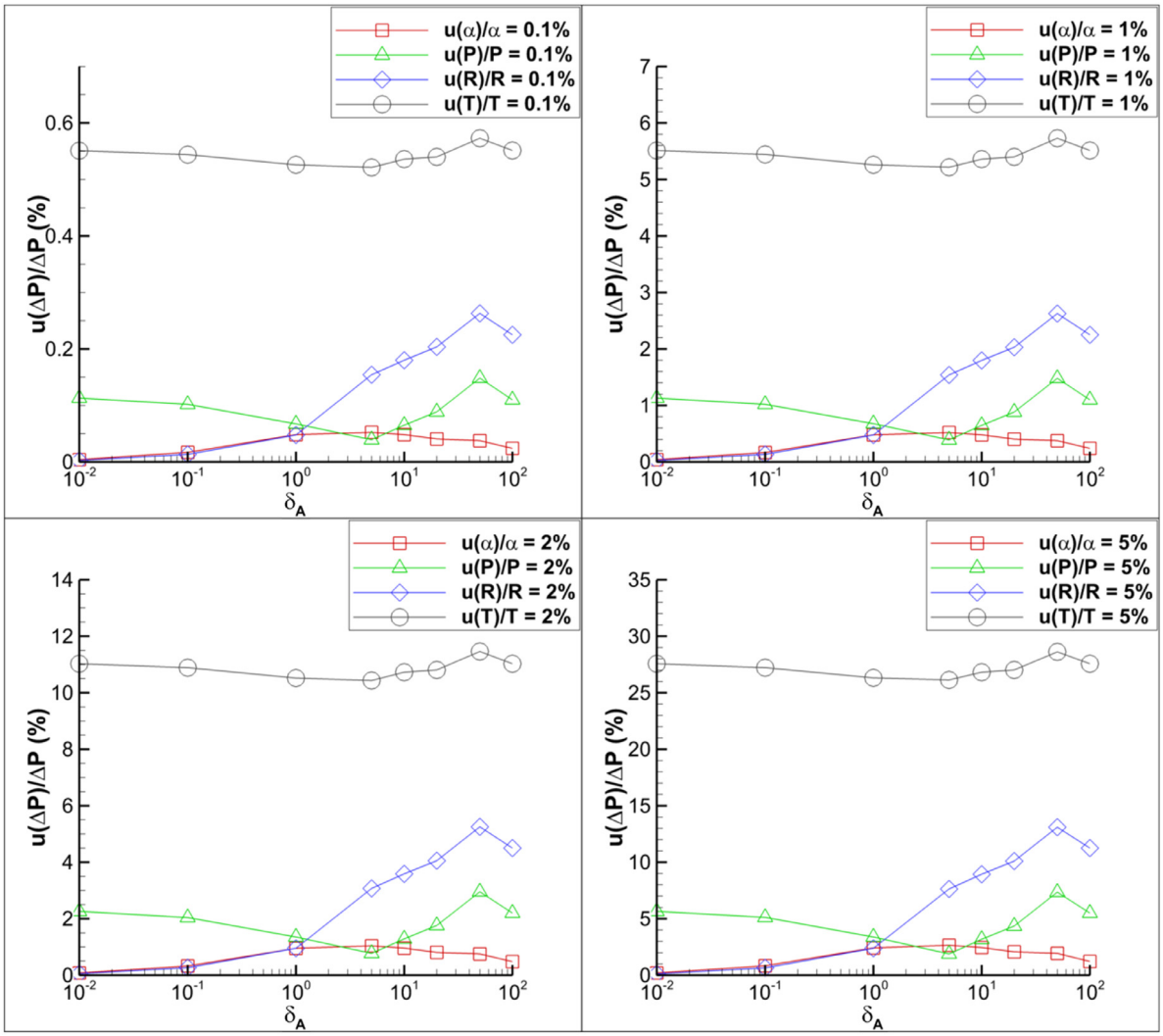

Fig. 5. Uncertainty $u(\Delta P)/\Delta P$ of the output pressure difference in the TPD flow in terms of δ_A, with the uncertainty in the input quantities of radius $u(R)/R$, pressure $u(P)/P$, temperature $u(T)/T$ and accommodation coefficient $u(\alpha)/\alpha$ equal, in each case, to 0.1%, 1%, 2% and 5%.

4.2. Uncertainty of pressure difference in TPD flow

Next, the thermomolecular pressure difference flow, based on Eq. (4), is considered. Simulations have been conducted in a wide range of δ_A, ranging from the free molecular up to the continuum regimes, analyzing the effect of the uncertainties in main input quantities of pressure, temperature, radius and accommodation coefficient on the uncertainty $u(\Delta P)/\Delta P$ of the generated pressure difference ΔP. It is noted that the TPD flow results are independent of the length of tube (see Eq. (4)) and therefore, the uncertainty in the tube length is not considered. The effect of the nominal input temperature ratio $T_{B,n}/T_{A,n}$ on the pressure difference uncertainty is also investigated. The input uncertainty in temperatures T_A and T_B are both of the same level but their values are sampled individually, while the pressure uncertainty has an effect only on the inlet pressure (the outlet pressure is an output quantity). The ratio of the length over the nominal radius of the tube is $L/R_n = 20$ and the nominal accommodation coefficient is $\alpha_n = 1$.

The relative uncertainty $u(\Delta P)/\Delta P$ of the output pressure difference in terms of δ_A is plotted in Fig. 5 for four values of the relative uncertainty in all main input quantities, with the nominal temperature ratio driving the flow equal to $T_{B,n}/T_{A,n} = 1.5$. More specifically, the presented results are for the uncertainties in pressure $u(P)/P$, temperature $u(T)/T$, radius $u(R)/R$ and accommodation coefficient $u(\alpha)/\alpha$ respectively, taking in each case, the values of 0.1%, 1%, 2% and 5%.

In all cases, as expected, larger uncertainties in the input quantities lead to larger uncertainties in the pressure difference. Clearly, the uncertainty in temperature, compared to all others, is by far the most dominant one, affecting most significantly the uncertainty in the output pressure difference. It is seen that in all cases $u(\Delta P)/\Delta P$ is magnified more than five times compared to the corresponding $u(T)/T$ in the input temperature. This uncertainty magnification remains about the same in the whole range of gas rarefaction. The uncertainties in pressure and radius do not affect significantly the uncertainty in the pressure difference. With regard to the pressure uncertainty, as δ_A is increased, $u(\Delta P)/\Delta P$ is initially decreased reaching some minimum around $\delta_A = 5$, then it is increased up to some maximum and finally, at large values of δ_A is slightly decreased. This rather complicated behavior is attributed to the dependency of the kinetic coefficients G_P and G_T, as well as of their ratio G_T/G_P, introduced in Eq. (4) of the TPD flow, on the pressure through the gas rarefaction parameter. Approximately, in the whole range of δ_A, the output $u(\Delta P)/\Delta P$ is about the same with the input $u(P)/P$. With regard to the radius uncertainty, as δ_A is increased, $u(\Delta P)/\Delta P$ is initially negligible and then it is increased up to

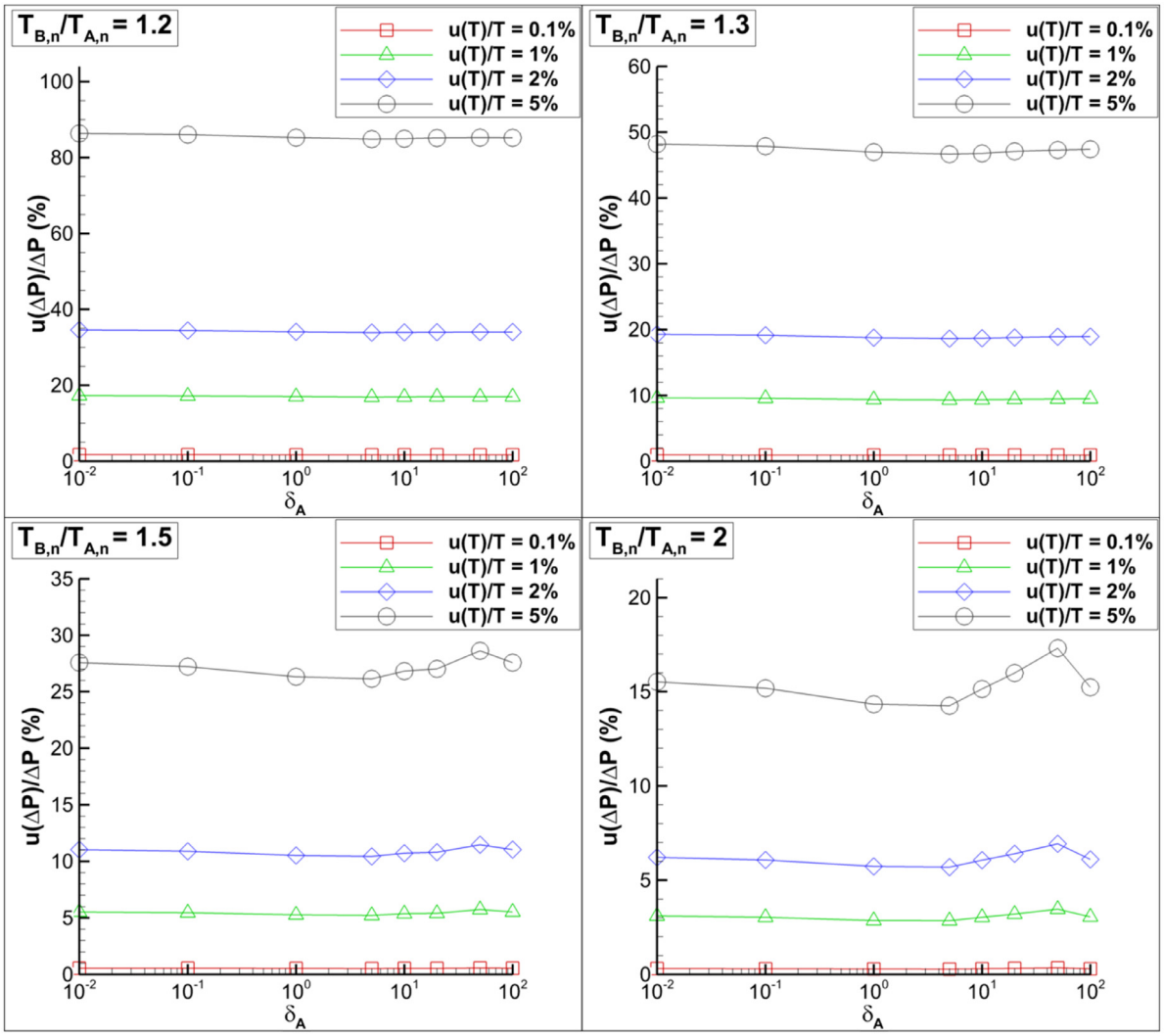

Fig. 6. Uncertainty $u(\Delta P)/\Delta P$ of the output pressure difference in the TPD flow in terms of δ_A for $T_{B,n}/T_{A,n} = 1.2$, 1.3, 1.5 and 2, with the uncertainty in the input temperatures $u(T)/T = 0.1\%$, 1%, 2% and 5%.

$\delta_A = 50$, where it is about two times larger than $u(R)/R$ and finally, it is slightly decreased. For $\delta_A < 1$ the pressure uncertainty is the second important one, followed by the radius uncertainty and for $\delta_A > 1$ the situation is reversed. As in the Poiseuille flow, the uncertainty in the accommodation coefficient of the Maxwell boundary conditions in the TPD flow, is less important compared to all others, with the output $u(\Delta P)/\Delta P$ being always abated compared to the corresponding input $u(\alpha)/\alpha$. It is interesting to note however, that when accommodation coefficient uncertainties are considered, contrary to the Poiseuille flow, $u(\Delta P)/\Delta P$ exhibits a peak in the transition regime, while the corresponding uncertainties in the free molecular and continuum regimes take very small values. This unexpected behavior is attributed to the fact that although in small values of δ_A the accommodation coefficient has a more considerable effect on each of the kinetic coefficients G_P and G_T, their ratio is much less affected, while in the transition regime their ratio is more affected. The maximum values of the pressure difference uncertainties for 5% uncertainty in temperature, radius, pressure and accommodation coefficient, are about 28%, 13%, 7% and 3% respectively. It is noted that similarly to the mass flow rate uncertainty in the Poiseuille flow, the relative uncertainty in the generated pressure difference in the TPD flow increases linearly with the relative uncertainty in the input quantities.

Furthermore, since the TPD flow is a thermally driven flow, the effect of the input temperature ratio on the uncertainty of the output pressure difference is investigated. In Fig. 6, the relative uncertainty $u(\Delta P)/\Delta P$ of the pressure difference in terms of δ_A is plotted for nominal temperature ratios $T_{B,n}/T_{A,n} = 1.2$, 1.3, 1.5 and 2, with the input uncertainty in temperature $u(T)/T$ taking the values of 0.1%, 1%, 2% and 5%. As the nominal temperature ratio is decreased, i.e., the temperature difference is also decreased, the output uncertainty $u(\Delta P)/\Delta P$ due to the input uncertainty $u(T)/T$ is drastically magnified. The values of the pressure difference uncertainty for 5% uncertainty in temperature reach up to 17%, 28%, 48% and 85% for temperature ratios 2, 1.5, 1.3 and 1.2 respectively. Also, as the temperature ratio decreases, the uncertainty in the pressure difference due to the temperature uncertainty becomes independent of δ_A. In the TPD flow the input temperature uncertainty is always the one which mostly affects the output pressure difference uncertainty and this effect becomes even more dominant as the temperature difference driving the flow is decreased.

4.3. Uncertainty of mass flow rate in thermal creep flow

Finally, the thermal creep flow, based on Eq. (1) subject to equal end pressures, is considered. As in the other two flows,

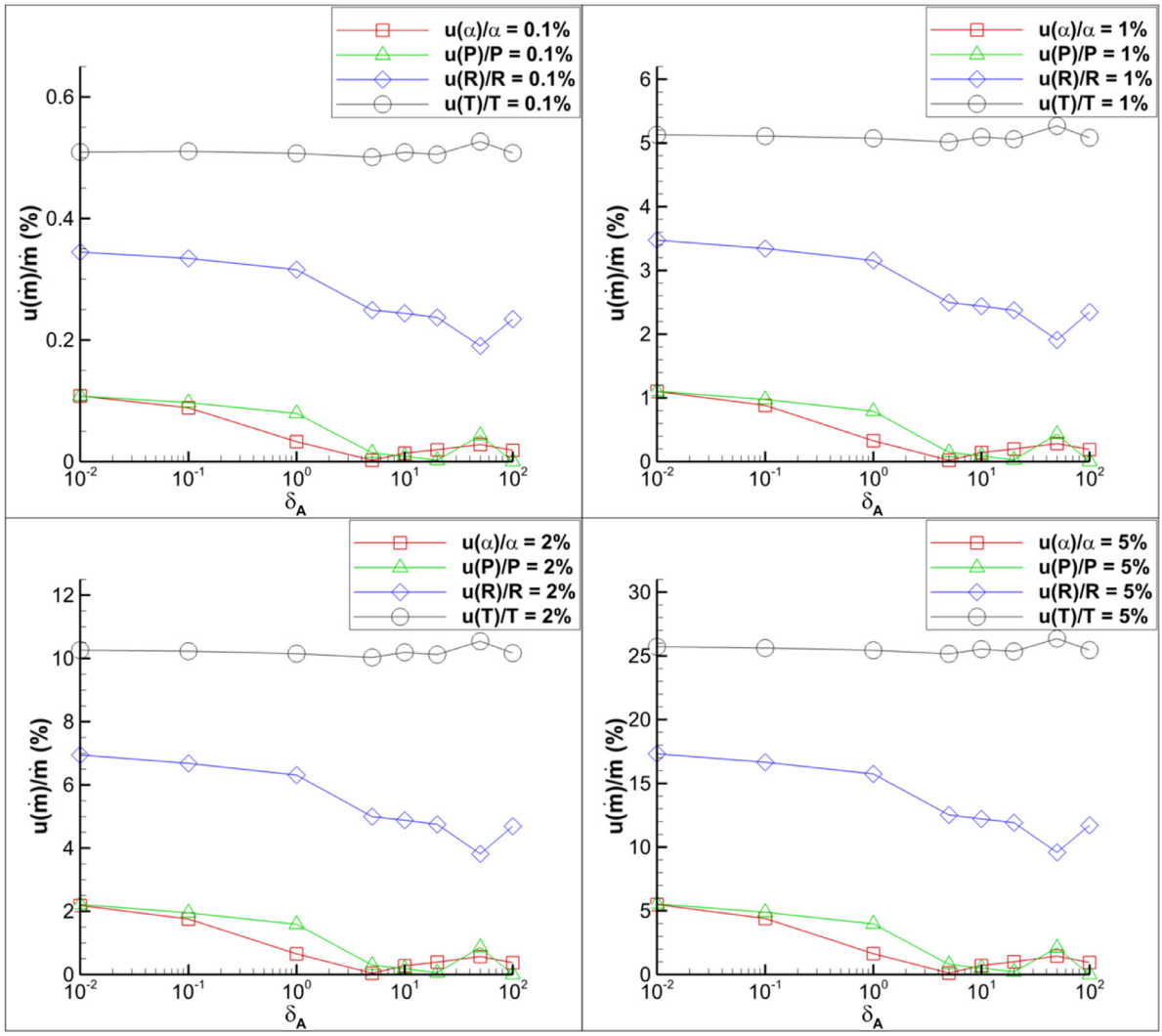

Fig. 7. Uncertainty $u(\dot{m})/\dot{m}$ of the output mass flow rate in the thermal creep flow in terms of δ_A, with the uncertainty in the input quantities of radius $u(R)/R$, pressure $u(P)/P$, temperature $u(T)/T$ and accommodation coefficient $u(\alpha)/\alpha$ equal, in each case, to 0.1%, 1%, 2% and 5%.

simulations have been conducted in a wide range of δ_A analyzing the effect of the uncertainty in the input quantities of pressure, temperature, radius, length and accommodation coefficient on the uncertainty in the output mass flow rate. The effect of the temperature ratio driving the flow on the uncertainty in the mass flow rate due to the temperature uncertainty is also investigated. Both temperatures T_A and T_B are subject to the same level of uncertainty but their values are sampled independently. Also, a single value is sampled for both $P_A = P_B$ in order to maintain a vanishing pressure difference. Concerning the effect of tube length uncertainty it is readily shown that it is the same as in the Poiseuille flow, i.e. $u(\dot{m})/\dot{m}$ it is directly proportional to $u(L)/L$.

Next, the relative uncertainty $u(\dot{m})/\dot{m}$ of the output mass flow rate in terms of δ_A is plotted in Fig. 7 for the input uncertainties $u(P)/P$, $u(T)/T$, $u(R)/R$ and $u(\alpha)/\alpha$, taking in each case, the values of 0.1%, 1%, 2% and 5%, with $T_{B,n}/T_{A,n} = 1.5$, $L/R_n = 20$ and $\alpha_n = 1$. As in the TPD flow the input uncertainty $u(T)/T$ is the one mostly affecting the output uncertainty $u(\dot{m})/\dot{m}$, which is more than five times higher compared to the corresponding introduced $u(T)/T$ and this magnification remains about constant in the whole range of gas rarefaction. Unlike in the TPD flow, the second important input parameter is clearly the radius followed by the pressure, which now has about the same influence with the accommodation coefficient. As it is seen, the uncertainty $u(\dot{m})/\dot{m}$ is about three times higher than $u(R)/R$, while it is about the same or even smaller than $u(P)/P$ and $u(\alpha)/\alpha$. With respect to the gas rarefaction parameter, as δ_A is increased, the output mass flow rate uncertainties due to the input radius, pressure and accommodation coefficient uncertainties are, in general, reduced. The maximum values of the mass flow rate uncertainties for 5% uncertainty in temperature, radius, pressure and accommodation coefficient, are about 26%, 17%, 5% and 5% respectively. Based on Fig. 7, it is deduced that as in the Poiseuille and TPD flows for the mass flow rate and pressure difference respectively, in the thermal creep flow the relative uncertainty in the mass flow rate increases linearly with the relative uncertainty in the input quantities.

In Fig. 8, the relative uncertainty $u(\dot{m})/\dot{m}$ of the mass flow rate in terms of δ_A is plotted for nominal temperature ratios $T_{B,n}/T_{A,n} = 1.2$, 1.3, 1.5 and 2, with the input uncertainty in temperature $u(T)/T$ taking the values of 0.1%, 1%, 2% and 5%. The dimensionless length is $L/R_n = 20$ and the accommodation coefficient is $\alpha_n = 1$. It is interesting to note that the results in Fig. 8 for the mass flow rate uncertainty are both qualitatively and quantitatively very close to the corresponding ones in Fig. 6 for the pressure difference uncertainty. Thus, as the nominal temperature ratio is decreased, the output uncertainty $u(\dot{m})/\dot{m}$ due to the input uncertainty $u(T)/T$, is drastically increased

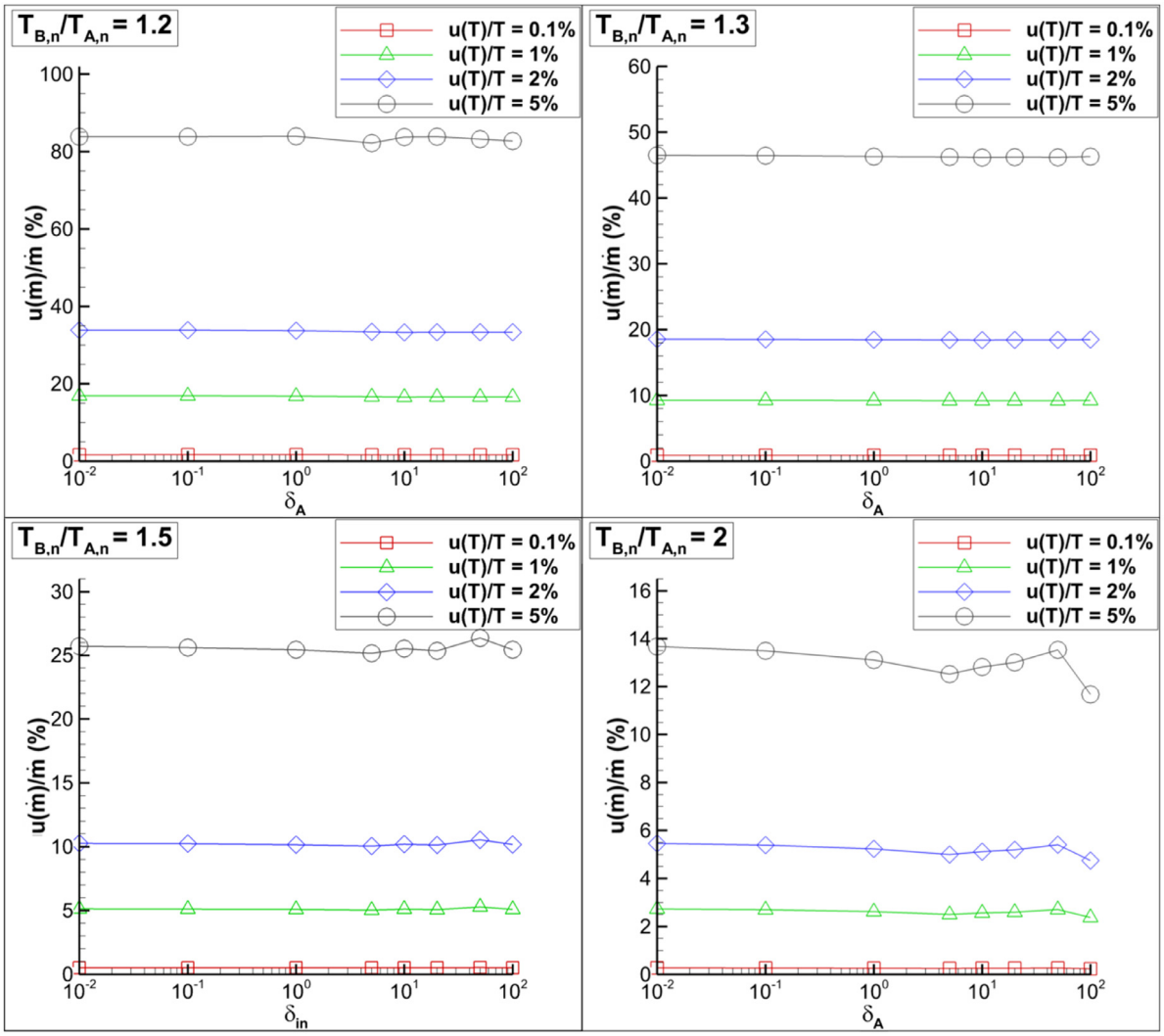

Fig. 8. Uncertainty $u(\dot{m})/\dot{m}$ of the output mass flow rate in the thermal creep flow in terms of δ_A for $T_{B,n}/T_{A,n} = 1.2$, 1.3, 1.5 and 2, with the uncertainty in the input temperatures $u(T)/T = 0.1\%$, 1%, 2% and 5%.

(similar to $u(\Delta P)/\Delta P$). Additionally, the values of the mass flow rate uncertainty for 5% uncertainty in temperature reach up to 14%, 26%, 47% and 85% for temperature ratios 2, 1.5, 1.3 and 1.2 respectively, which are very close to the corresponding pressure difference uncertainties reported in Fig. 6. It may be stated that in the thermal creep flow the input temperature uncertainty is always the one affecting mostly the output mass flow rate uncertainty and this is becoming even more dominant as the temperature difference driving the flow is decreased. Furthermore, making a qualitative comparison between the mass flow rate uncertainties, due to temperature uncertainty for $T_{B,n}/T_{A,n} = 2$ shown in Fig. 8 and due to radius uncertainty for $T_{B,n}/T_{A,n} = 1.5$, shown in Fig. 7, it is seen that they are about the same. Thus, in adequately large temperature differences and for relatively small values of δ_A, the radius uncertainty may overcome the temperature uncertainty and become the leading source of uncertainty.

5. Concluding remarks

The effect of the uncertainties which may be introduced in the input data on the uncertainty in the output quantities in classical rarefied gas flows is investigated. More specifically, the fully developed Poiseuille, thermomolecular pressure difference (TPD) and thermal creep flows through circular capillaries are considered. The input quantities include the length and the radius of the tube, the pressure and temperature at the capillary ends and the gas-surface accommodation coefficient and the introduced uncertainties are, for each parameter, equal to 0.1%, 1%, 2% and 5%. The propagation of the uncertainties through the computational model is performed via the Monte Carlo Method by conducting an adequate number of trials and the resulting uncertainty in the output mass flow rate and pressure difference are obtained.

In the Poiseuille flow driven by moderate and large pressure differences, the radius uncertainty is the most important one, resulting to an output mass flow rate uncertainty magnified about four times compared to the input radius uncertainty. However, in flows driven by relatively small pressure differences the pressure uncertainty becomes the dominant one mostly affecting the mass flow rate. In Poiseuille flow driven by a pressure ratio of 0.9, an input pressure uncertainty of 5% yields an output mass flow rate uncertainty of 42%.

In the TPD flow, independent of the magnitude of the temperature difference driving the flow, the temperature uncertainty is always, by far, the most important one, with the output pressure difference uncertainty magnified about five times compared to the input temperature uncertainty for a temperature ratio

driving the flow of 1.5. When the temperature ratio is reduced the uncertainty magnification is further increased. Indicatively, a temperature ratio of 1.2 yields an output uncertainty of the pressure difference up to 85% for an input temperature uncertainty of 5%.

In the thermal creep flow driven by small and moderate temperature differences, the input temperature uncertainty is clearly the most important one, magnifying the output mass flow rate uncertainty about five times compared to the input temperature uncertainty. However, for large temperature differences, the input radius uncertainty becomes more important.

Overall, it may be concluded that in most cases, the uncertainty in the input quantity driving the phenomenon, i.e., the pressure for the Poiseuille flow and the temperature for the TPD and thermal creep flows, is the most important source of uncertainty. This is always true in the TPD flow and for small driving thermodynamic forces in the other two flows. For large pressure and temperature differences driving the Poiseuille and thermal creep flows respectively, the radius becomes the most important source of uncertainty. As the force driving the flow is decreased the uncertainty in the main output quantity, due to the uncertainties in the driving force, becomes independent of the gas rarefaction parameter. Finally, the uncertainty in the accommodation coefficient of the Maxwell diffuse-specular boundary conditions is always the less important one. It has been also seen that in all cases the relative uncertainty in the output quantity grows linearly with the relative uncertainty in the input ones.

The presented results may be of great help in the comparison between computational and experimental work, particularly when inverse engineering practices are involved, as well as in the design of experimental rigs including the specification of the measuring devices in the field of rarefied gas dynamics. Having documented the expected effect of the uncertainty in each input parameter on the uncertainty in the output computed or measured quantity, may be beneficial in determining the range of operating conditions in order to improve the resolution of the observed phenomenon. The Monte Carlo Method for the uncertainty propagation implemented in the present work can be also applied in a broader range of more complex rarefied gas flows in an effort to support researchers and engineers engaged in the design of systems with miniaturized sizes and/or operating in low pressure conditions.

Acknowledgments

This work has been carried out within the framework of the EUROfusion Consortium and has received funding from the Euratom research and training program 2014–2018 and 2019–2020 under grant agreement No 633053 (WP EDU). The views and opinions expressed herein do not necessarily reflect those of the European Commission.

References

[1] P.J. Roache, Quantification of uncertainty in computational fluid dynamics, Annu. Rev. Fluid Mech. 29 (1) (1997) 123–160.
[2] L. Mathelin, M. Yousuff Hussaini, T.A. Zang, Stochastic approaches to uncertainty quantification in CFD simulations, Numer. Algorithms 38 (1–3) (2005) 209–236.
[3] H.W. Coleman, F. Stern, Uncertainties and CFD code validation, J. Fluids Eng. 119 (4) (1997) 795–803.
[4] H.W. Coleman, W.G. Steele, Engineering applications of experimental uncertainty analysis, AIAA J. 33 (10) (1995) 1888–1896.
[5] H.W. Coleman, W.G. Steele, Experimentation, Validation, and Uncertainty Analysis for Engineers, John Wiley & Sons, 2018.
[6] R.J. Moffat, Describing the uncertainties in experimental results, Exp. Therm. Fluid Sci. 1 (1) (1988) 3–17.
[7] J. Pitakarnnop, S. Varoutis, D. Valougeorgis, S. Geoffroy, L. Baldas, S. Colin, A novel experimental setup for gas microflows, Microfluid. Nanofluid. 8 (1) (2010) 57–72.
[8] E. Silva, C.J. Deschamps, M. Rojas-Cardenas, C. Barrot-Lattes, L. Baldas, S. Colin, A time-dependent method for the measurement of mass flow rate of gases in microchannels, Int. J. Heat Mass Transfer 120 (2018) 422–434.
[9] T. Ewart, P. Perrier, I. Graur, J.G. Meolans, Mass flow rate measurements in gas micro flows, Exp. Fluids 41 (3) (2006) 487–498.
[10] M. Rojas-Cardenas, I. Graur, P. Perrier, J.G. Meolans, Time-dependent experimental analysis of a thermal transpiration rarefied gas flow, Phys. Fluids 25 (7) (2013) 072001.
[11] A. Agrawal, S.V. Prabhu, Survey on measurement of tangential momentum accommodation coefficient, J. Vac. Sci. Technol. A 26 (4) (2008) 643–645.
[12] X. Guo, J. Li, D. Xiu, A. Alexeenko, Uncertainty quantification models for micro-scale squeeze-film damping, Internat. J. Numer. Methods Engrg. 84 (10) (2010) 157–1272.
[13] A. Alexeenko, M. Kulakhmetov, Modeling uncertainties in direct simulation Monte Carlo calculations of hypersonic leading-edge flow, J. Spacecr. Rockets 49 (3) (2012) 461–473.
[14] M. Kulakhmetov, A. Alexeenko, Model uncertainties in a sharp leading-edge hypersonic boundary, in: 49th AIAA Aerospace Sciences Meeting Including the New Horizons Forum and Aerospace Exposition, 2011.
[15] L. Kuckert, F. Heizmann, G. Drexlin, F. Glück, M. Hötzel, M. Kleeseik, F. Sharipov, K. Valerius, Modeling of gas dynamical properties of the KATRIN tritium source and implications for the neutrino mass measurement, Vacuum 158 (2018) 195–205.
[16] S. Naris, N. Vasileiadis, D. Valougeorgis, A.S. Hashad, W. Sabuga, Computation of the effective area and associated uncertainties of non-rotating piston gauges FPG and FRS, Metrologia 56 (1) (2008) 015004.
[17] F. Sharipov, Y. Yang, J.E. Ricker, J.H. Hendricks, Primary pressure standard based on piston-cylinder assemblies. Calculation of effective cross sectional area based on rarefied gas dynamics, Metrologia 53 (5) (2016) 1177.
[18] M. Lorenzini, G.L. Morini, T. Henning, J. Brandner, Uncertainty assessment in friction factor measurements as a tool to design experimental set-ups, Int. J. Therm. Sci. 48 (2009) 282–289.
[19] G.L. Morini, M. Lorenzini, M. Spiga, A criterion for experimental validation of slip-flow models for incompressible rarefied gases through microchannels, Microfluid. Nanofluid. 1 (2) (2005) 190–196.
[20] M. Lorenzini, G.L. Morini, T. Henning, J. Brandner, Experimental uncertainties analysis as a tool for friction factor determination in microchannels, Proc. Inst. Mech. Eng. C 222 (5) (2008) 817–827.
[21] R.W. Walters, L. Huyse, Uncertainty Analysis for Fluid Mechanics with Applications, No. ICASE-2002-1 National Aeronautics and Space Administration, Hampton VA Langley Research Center, 2002.
[22] M.G. Morgan, M. Henrion, M. Small, Uncertainty: A Guide to Dealing with Uncertainty in Quantitative Risk and Policy Analysis, Cambridge University Press, 1992.
[23] R.E. Moore, Methods and Applications of Interval Analysis, Vol. 2, SIAM, 1979.
[24] M.M. Putko, A.C. Taylor, P.A. Newman, L.L. Green, Approach for input uncertainty propagation and robust design in CFD using sensitivity derivatives, J. Fluids Eng. 124 (1) (2002) 60.
[25] L. Huyse, Solving problems of optimization under uncertainty as statistical decision problems, in 19th AIAA Applied Aerodynamics Conference, 2001, p. 1519.
[26] O.M. Knio, O.P. Le Maitre, Uncertainty propagation in CFD using polynomial chaos decomposition, Fluid Dyn. Res. 38 (9) (2006) 616–640.
[27] J.M. Hammersley, D.C. Handscomb, Monte Carlo Methods, in: Methuen's Monographs on Applied Probability and Statistics, Metheun, London, 1964.
[28] F. Sharipov, V. Seleznev, Rarefied gas flow through a long tube at any pressure ratio, J. Vac. Sci. Technol. A 12 (5) (1994) 2933–2935.
[29] F. Sharipov, Rarefied gas flow through a long tube at any temperature ratio, J. Vac. Sci. Technol. A 14 (4) (1996) 2627–2635.
[30] N. Vasileiadis, G. Tatsios, S. Misdanitis, D. Valougeorgis, Modeling of complex gas distribution systems operating under any vacuum conditions: Simulations of the ITER divertor pumping system, Fusion Eng. Des. 103 (2016) 125–135.
[31] V. Hauer, C. Day, Conductance modeling of ITER vacuum systems, Fusion Eng. Des. 84 (2–6) (2009) 903–907.
[32] M.V. Johansson, F. Testa, I. Zaier, P. Perrier, J.P. Bonnet, P. Moulin, I. Graur, Mass flow rate and permeability measurements in microporous media, Vacuum 158 (2018) 75–85.
[33] G. Tatsios, G. Lopez Quesada, M. Rojas-Cardenas, L. Baldas, S. Colin, D. Valougeorgis, Computational investigation and parametrization of the pumping effect in temperature-driven flows through long tapered channels, Microfluid. Nanofluid. 21 (5) (2017) 99.
[34] M. Gad-el-Hak, The MEMS Handbook, CRC Press, 2001.
[35] S. An, N.K. Gupta, Y.B. Gianchandani, A Si-micromachined 162-stage two-part Knudsen pump for on-chip vacuum, J. Microelectromech. Syst. 23 (2) (2014) 406–416.
[36] I. Graur, F. Sharipov, Non-isothermal flow of rarefied gas through a long pipe with elliptic cross section, Microfluid. Nanofluid. 6 (2) (2009) 267–275.

[37] F. Sharipov, V. Seleznev, Data on internal rarefied gas flows, J. Phys. Chem. Ref. Data 27 (3) (1998) 657.
[38] F. Sharipov, G. Bertoldo, Poiseuille flow and thermal creep based on the Boltzmann equation with the Lennard–Jones potential over a wide range of the Knudsen number, Phys. Fluids 21 (6) (2009) 067101.
[39] L. Wu, H. Struchtrup, Assessment and development of the gas kinetic boundary conditions for the Boltzmann equation, J. Fluid Mech. 823 (2017) 511–537.
[40] ISO, IEC, BIPM OIML, Guide to the Expression of Uncertainty in Measurement, Geneva, Switzerland, 1995.
[41] BIPM, IEC, ILAC IFCC, IUPAC ISO, Evaluation of Measurement Data – Supplement 1 to the Guide to the Expression of Uncertainty in Measurement, Propagation of Distributions using a Monte Carlo Method, Joint Committee for Guides in Metrology, Vol. 101, Bureau International des Poids et Mesures, JCGM, 2008.